

Electronic Supplementary Information

Iridium on vertical graphene as an all-round catalyst for robust water splitting reactions

Sanjib Baran Roy^a, Kamran Akbar^b, Jae Ho Jeon^a, Sahng-Kyoong Jerng^c, Linh Truong^a, Kiwoong Kim^d, Yeonjin Yi^d, and Seung-Hyun Chun^{a,*}

^aDepartment of Physics, Sejong University, Seoul 05006, Korea

^bDepartment of Energy Science, Sungkyunkwan University, Suwon 16419, Korea

^cGraphene Research Institute, Sejong University, Seoul 05006, Korea

^dInstitute of Physics and Applied Physics, Yonsei University, Seoul 03722, Korea

* Corresponding Author: FAX: +82 2 3408 4316. E-mail address: schun@sejong.ac.kr (S. H. Chun)

Experimental section:

Growth of the VG. VG was grown by PECVD. To remove unintended contaminants, GC substrate was treated by H₂ plasma with a radio frequency (RF) power of 50 W for 2 min under a H₂ flow rate of 20 standards cubic centimetre per min (sccm). After this treatment, methane (CH₄, 10 sccm) and H₂ (20 sccm) were discharged using an RF power of 50 W for 45 min at 750 °C for VG growth. Further details can be found elsewhere.¹

Deposition of Ir. High purity Ir (99.99 %, Alfa Aesar) was deposited by an e-beam evaporation technique. Solid Ir was sublimated from an alumina crucible in a high-vacuum chamber. During the deposition process, the vacuum level was maintained at approximately 9x10⁻⁶ Torr. The nominal deposition rate, determined from the thickest film, was 1 nm/50 s. Atomic force microscopy (AFM) was used to measure the thickness of Ir.

Electrochemical measurements. All the electrochemical measurements were performed with various catalysts utilizing a typical three-electrode setup in 0.5 M H₂SO₄ and 1 M KOH at room temperature for HER and OER. The GC substrate served as the working electrode, a Ag/AgCl and Hg/HgO electrode was utilized as the reference electrode for acidic and alkaline electrolyte, respectively. To fill the circuit a graphite rod was used as counter electrode for both HER and OER. 20% Pt/C and IrO₂ deposited on GC served as standard reference for HER and OER, respectively. The HER /OER activity was evaluated by linear sweep voltammetry (LSV) with a scan rate of 10 mV s⁻¹ using an electrochemical workstation (Biologic SP-300, Biologic Science Instruments). The recorded potential values were converted to the reversible hydrogen electrode (RHE) scale according to the following equation, $E \text{ (RHE)}_{\text{AgCl}} = E \text{ (vs. Ag/AgCl)} + E^0_{\text{Ag/AgCl}} +$

$0.0592 \times \text{pH}$ and $E(\text{RHE})_{\text{HgO}} = E(\text{vs. Hg/HgO}) + E^0_{(\text{Hg/HgO})} + 0.0592 \times \text{pH}$. Polarization curves were collected after iR compensation in 0.5 M H_2SO_4 and 1 M KOH. The linear portions of Tafel plots were fitted to Tafel equation $\eta = a + b \log (j)$ for Tafel slope value b . The current density was calculated from the geometric working area of GC electrode ($\sim 0.30 \text{ cm}^2$). Electrochemical impedance spectroscopy (EIS) was tested at frequency range of 1 Hz \sim 1 MHz.

Other characterizations. Field emission scanning electron microscopy (FESEM) measurements were conducted using a Hitachi S4700 system (operated at 15 kV) with electron dispersive spectroscopy (EDS, Horiba EMAX) capability for elemental mapping. High-resolution transmission electron microscopy (HRTEM) measurements were performed using a JEM-2100F instrument (operated at 200 kV) with an Oxford EDS system. The surface morphology was obtained using a commercial AFM instrument (n-Tracer system, Nano Focus Inc.) operated in non-contact mode. Chemical bonds were analysed by X-ray photoelectron spectroscopy (XPS) with an Al $\text{K}\alpha$ source (1486.6 eV) line.

Turnover frequency (TOF): The turnover frequency (per Ir site) was calculated by assuming 100% faradaic efficiency with the following equation:

$$\text{TOF} = I / (4 \times F \times m)$$

Where, I = the current (A); F = Faraday constant; m = the number of moles in catalyst.

Mass Activity: Mass activity was calculated from the ratio between current density and loading catalyst mass;

Mass activity (A/ mg) = j / m ; at specific overpotential.

Where, j = current density; m = loading catalyst amount.

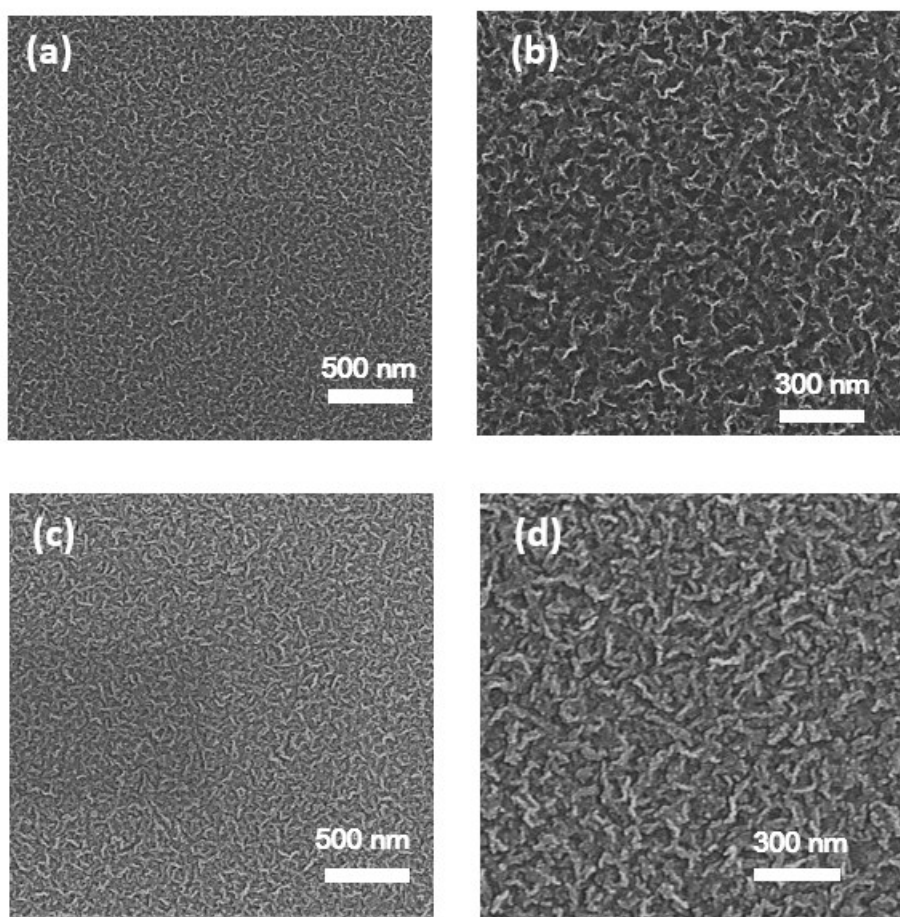


Fig. S1. FESEM images for Ir_GC at low (a) and high (b) magnification: Ir (10nm) on VG makes the graphene nanosheets broader which is distinguishable at low(c) and high (d) magnification.

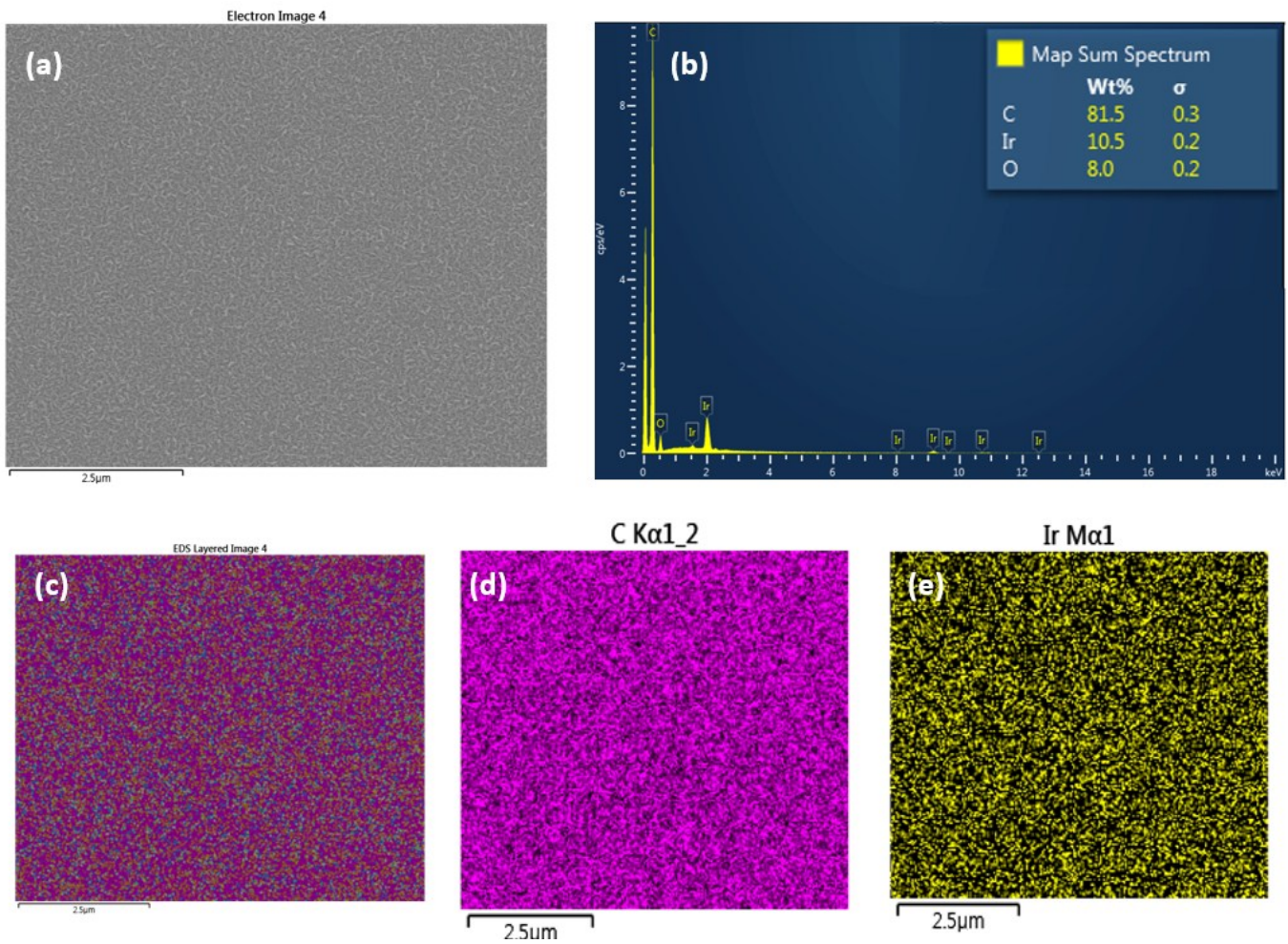


Fig. S2. EDX and elemental mapping: The EDX of as grown Ir_VG sample (a) shows in (b). The elemental mapping results are shown in (c – e).

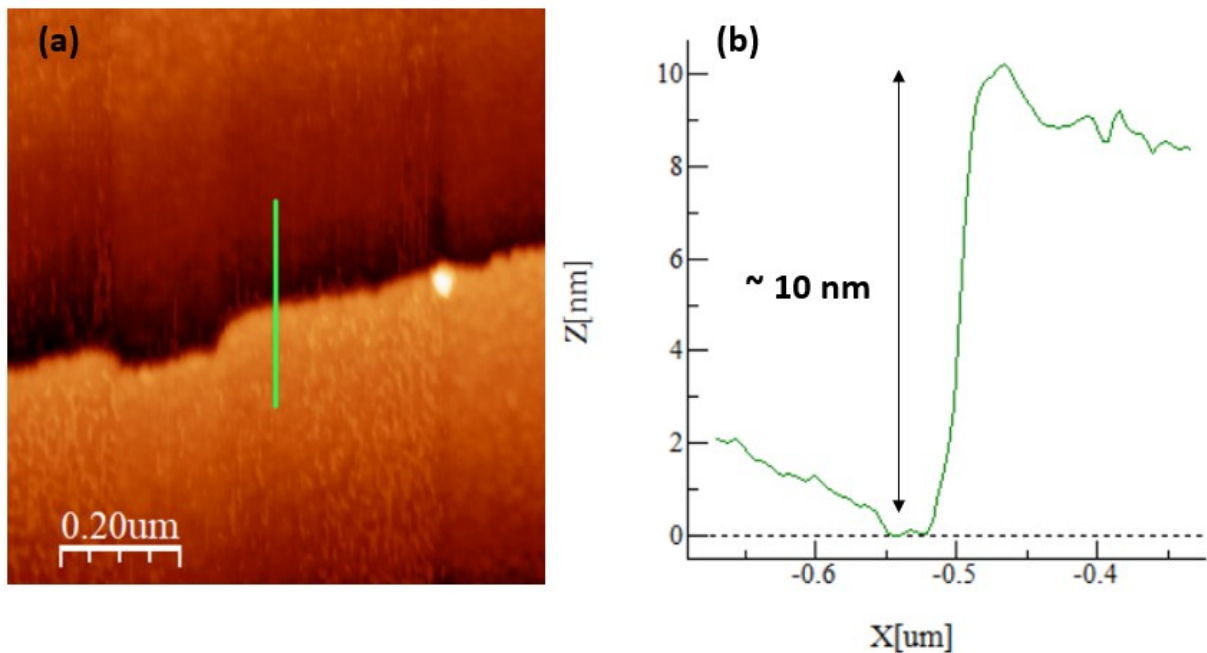


Fig. S3 Thickness of deposited Ir (10nm): AFM was employed to measure the exact thickness of e-beam evaporated Ir. It confirms almost 10 nm-thick Ir was deposited upon VG towards fabricate Ir_VG.

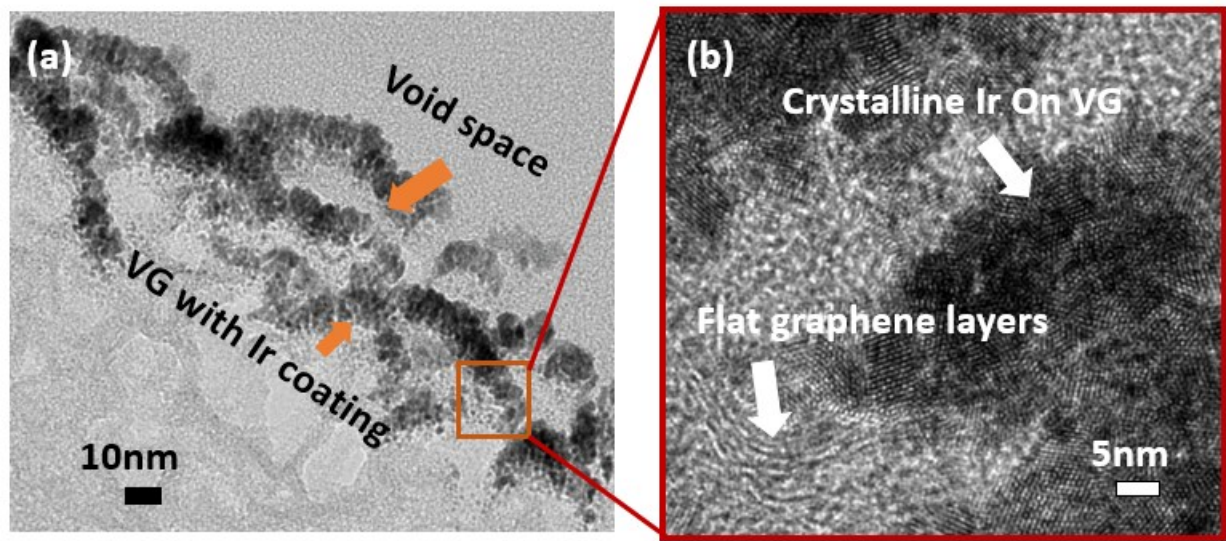


Fig. S4. HRTEM of Ir_VG: The different lateral position of Ir coated vertical graphene nanosheets with void space in between shown in (a). Magnified image of inside the box in (a) shown in (b); at bottom several flat graphene layers act as faster electron transfer channel. Highly crystalline Ir is clearly visible at top of VG sheets.

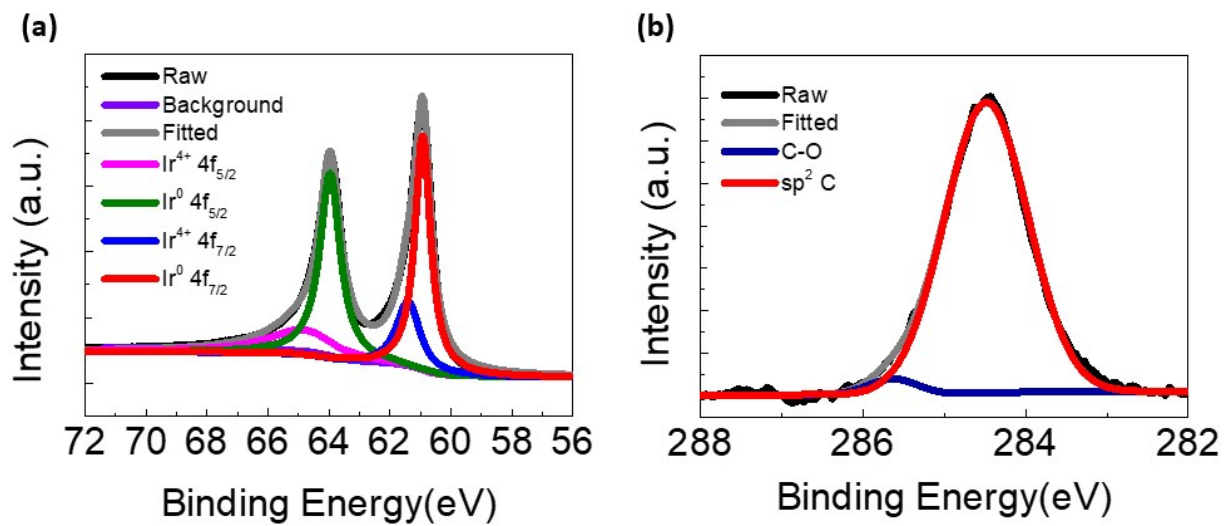


Fig. S5. XPS spectra of as grown Ir_VG: Metallic Ir is prominent than oxide contribution shown in (a). C=C bonding in C1s spectra comes from VG sheets (b). C-O bonding can be attributed to additional oxygen gain from environment after growth.

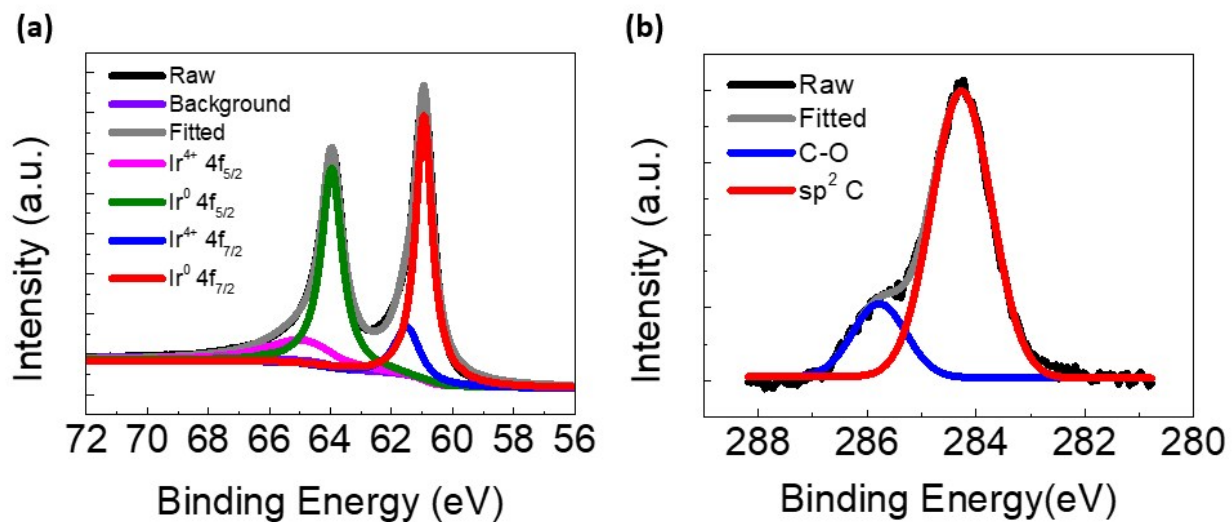


Fig. S6. XPS spectra of Ir_VG after 300 cycles of HER in 0.5 M H_2SO_4 : The metallic Ir is still dominant (a) and no increment of oxidized valance state of Ir was observed. C 1s (b) spectra shows slightly higher C-O bonding after 300 cycles compare to as grown sample.

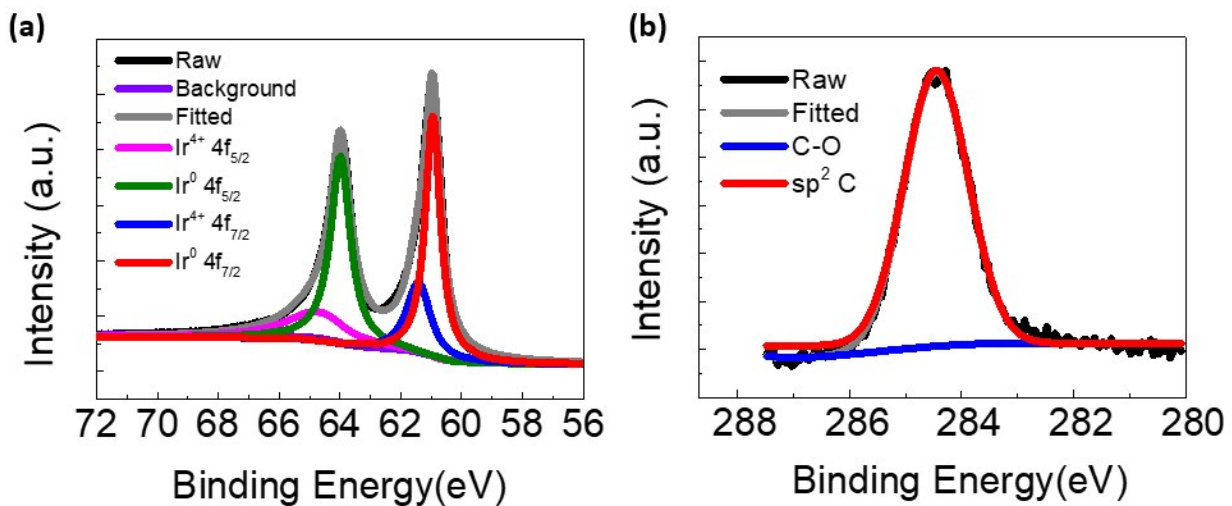


Fig. S7. XPS spectra of Ir_VG after 300 cycles of OER in 1 M KOH: After 300 cycles of anodic OER in KOH, Ir particle sustain as metallic state (a). No further C-O bonding was observed at C 1s spectra (b).

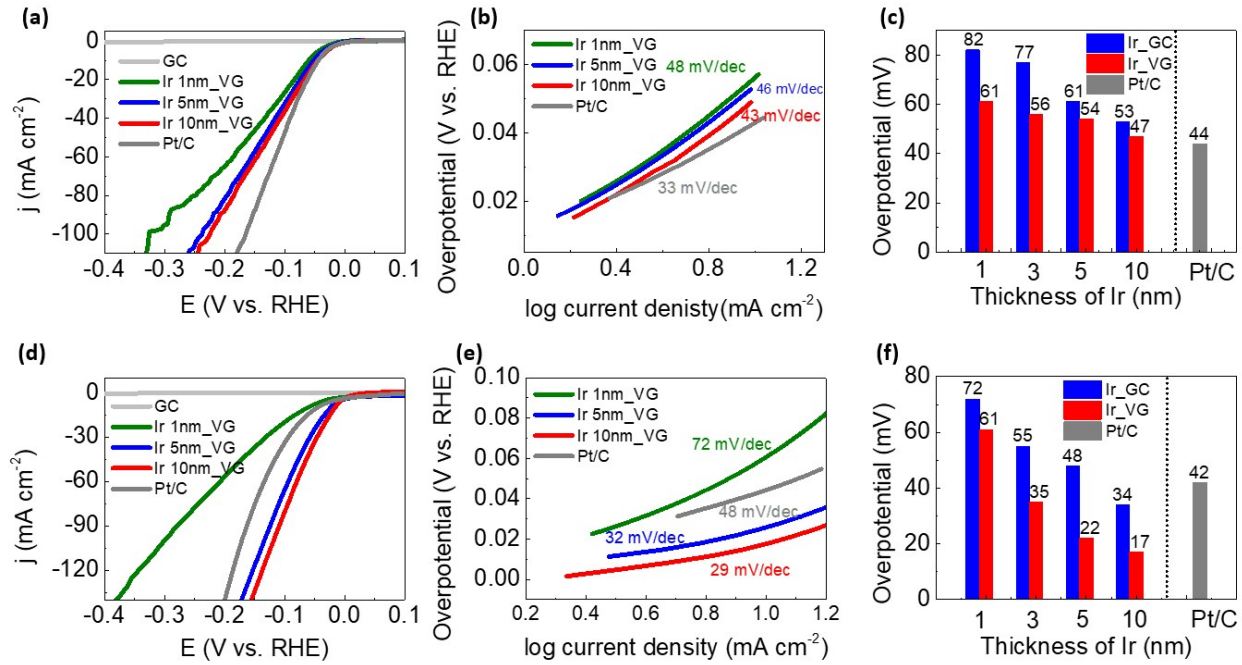


Fig. S8. HER performance in acid and base: With increasing thickness of Ir the HER performance becomes better in acid (a) and base (d). Ir(10nm)_VG shows lower Tafel slope of 43 mV/dec and 29 mV/dec in acid (d) and base (e) respectively. The superior catalytic activity of Ir_VG at 10mA/cm 2 than Ir_GC in both acid and base presents in (c) and (f) respectively.

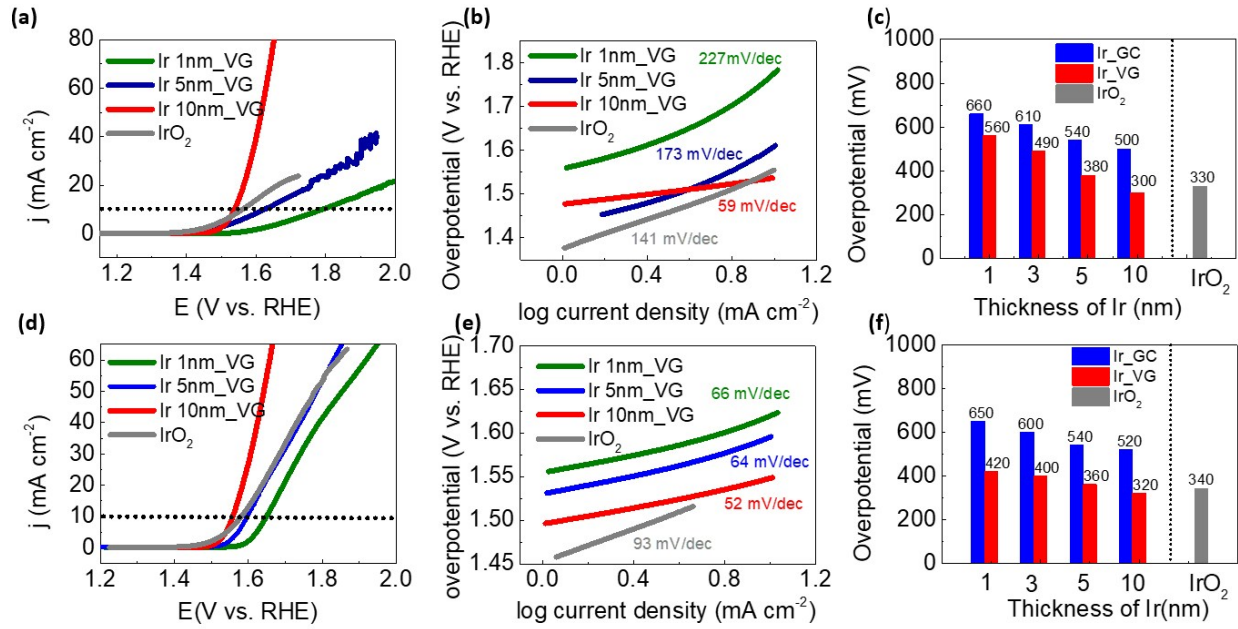


Fig. S9. OER performance in acid and base: Higher Ir content shows better OER activity with high current density at low applied potential in both acid (a) and base (d). Tafel slope goes lower for Ir(10nm)_VG in both acidic (b) and alkaline (e) medium. Even in sluggish OER, Ir_VG achieves lower overpotential at 10 mA/cm^2 than Ir_GC and IrO_2 in both acidic (c) and alkaline (f) medium.

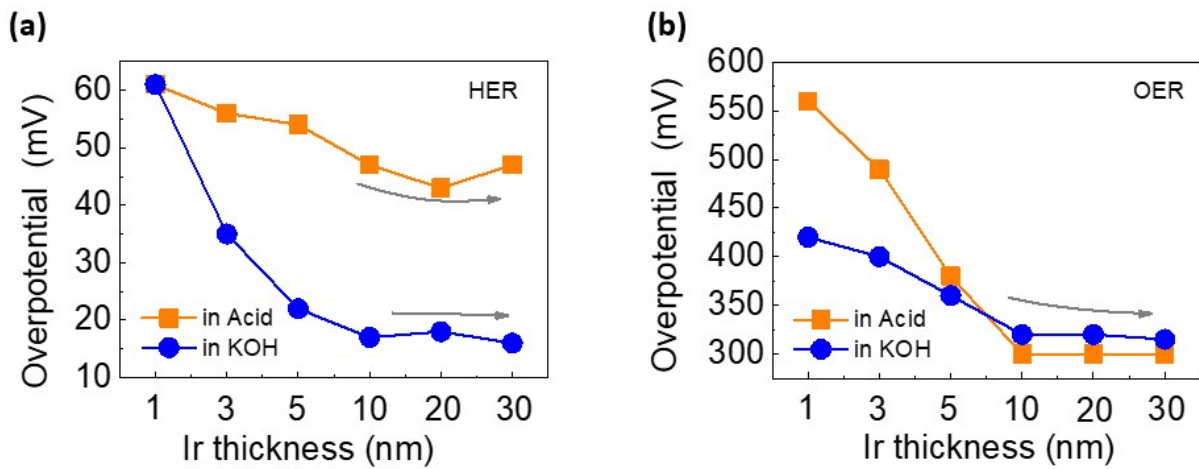


Fig. S10. Catalytic performance of thicker Iridium: At increasing Ir content (20,30nm) the catalytic performance shows a saturation like behavior in HER (a) and OER (b) which implies Ir (10nm) on VG is the optimum condition achieved in all four catalytic medium.

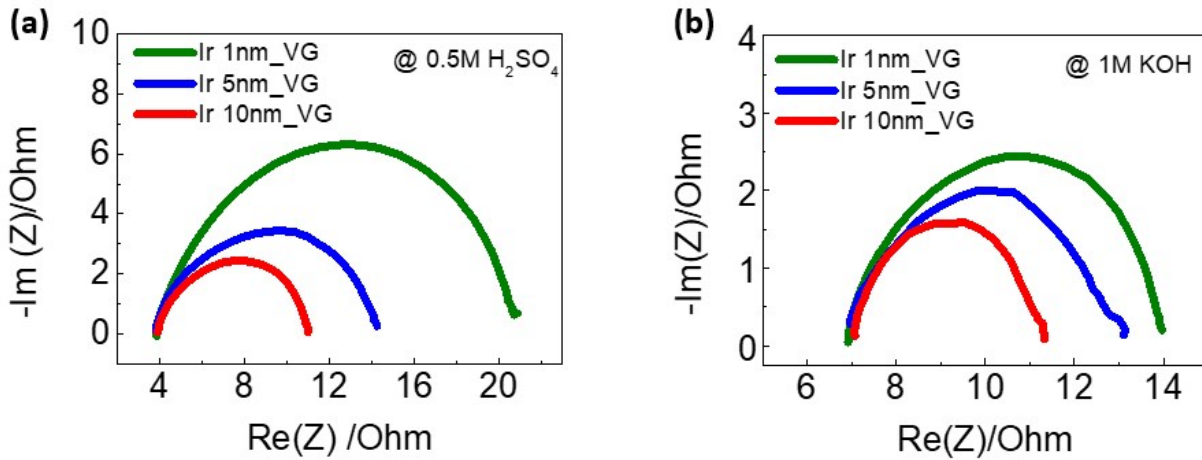


Fig. S11. EIS of Ir_VG hybrid: Ir (10nm)_VG shows less charge transfer resistance with compared to thinner Ir on VG. In both acidic (a) and alkaline (b) electrolyte the smallest semicircle was achieved for Ir (10nm)_VG in an AC impedance measurement for HER (at -0.4V vs RHE) and OER (at 1.6V vs RHE).

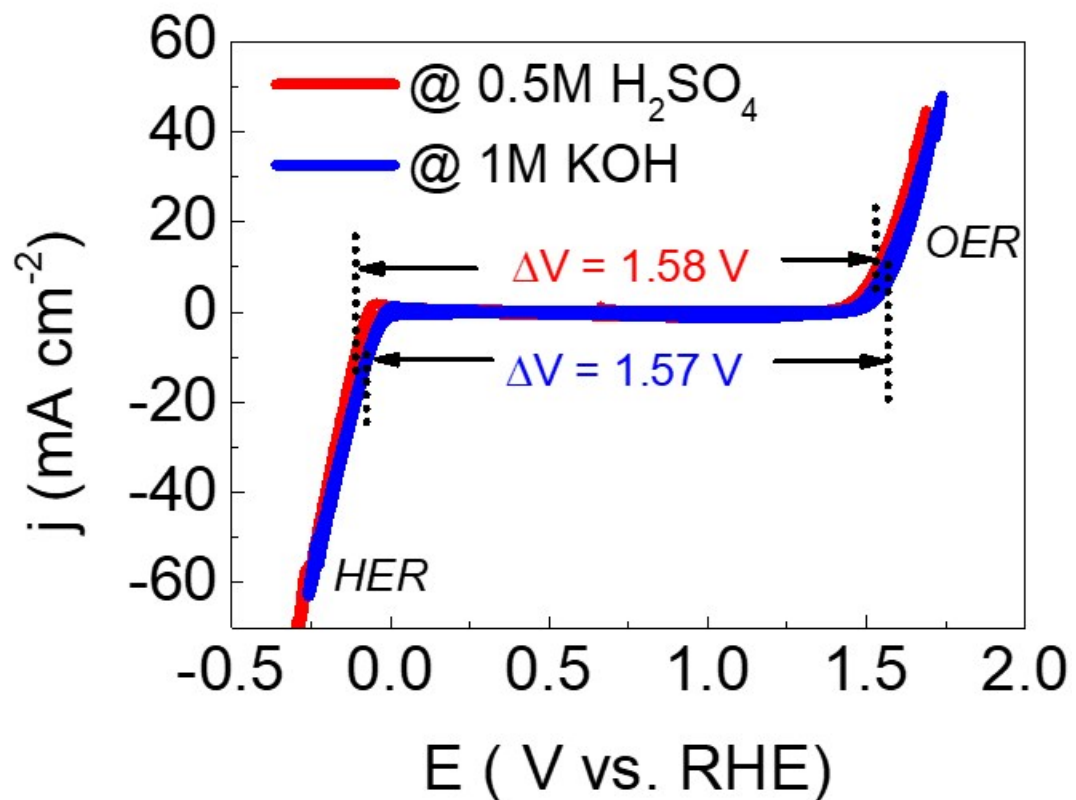


Fig. S12. Total Water Splitting reaction: Ir_VG hybrid performs efficiently as a cathodic and anodic material in overall water splitting reaction. In the total water splitting reaction window, Ir_VG shows a low voltage difference of 1.58 V (acid) and 1.57 V (alkaline) between HER and OER activation at a current density of 10 mA/cm^2 .

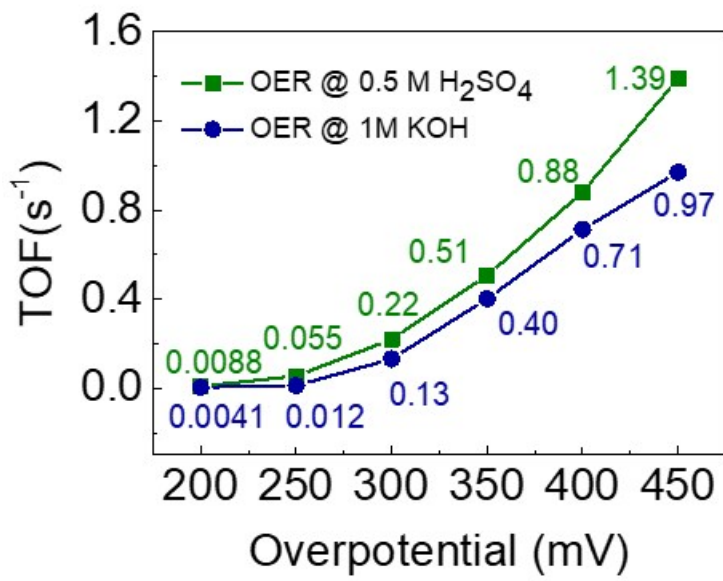


Fig. S13. The turnover frequency (TOF) of Ir_VG hybrid for OER in acid and alkaline at different overpotential, which is related to the O₂ gas production per Ir site can be comparable to some electrocatalysts.^{2,3}

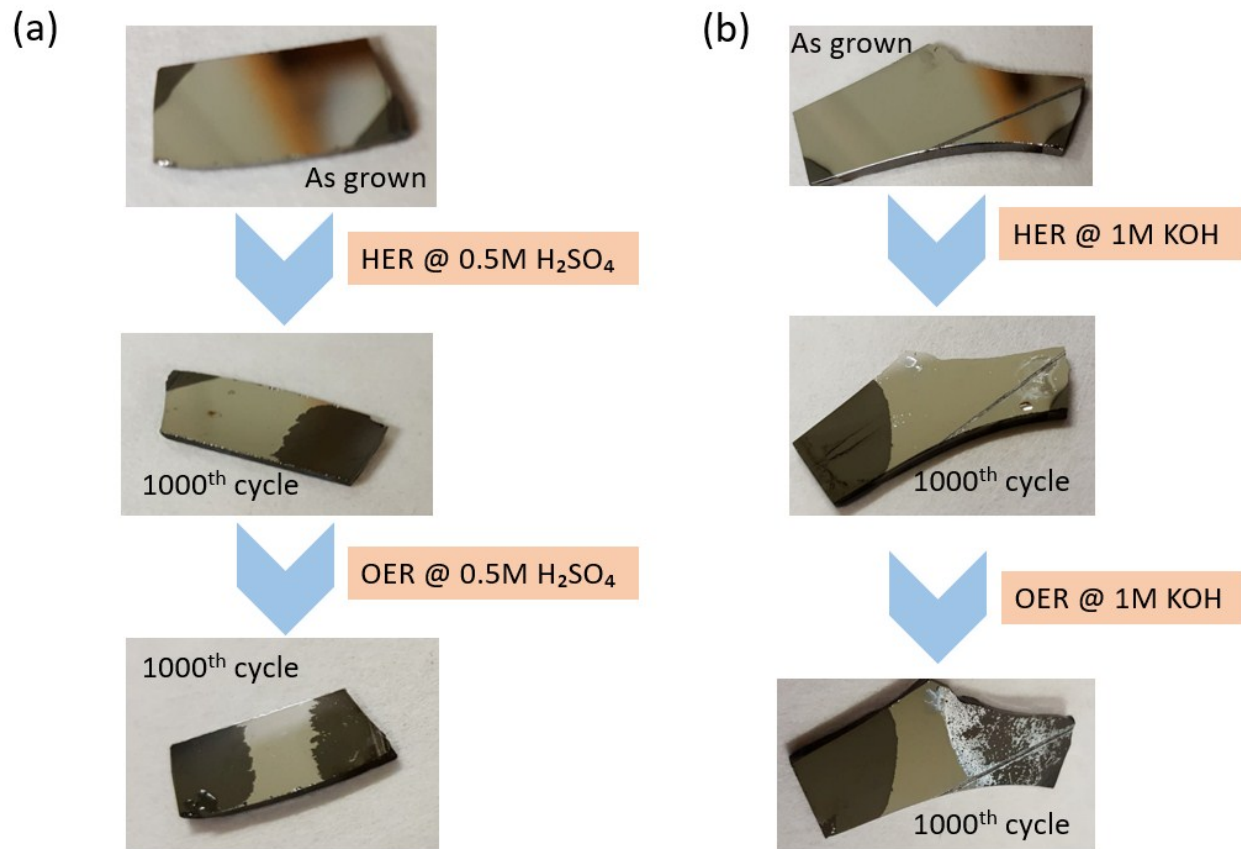


Fig. S14. The optical images represent the corrosiveness of Ir without VG. Without supporting VG, Ir was totally dissolved in acid (a) and alkaline (b).

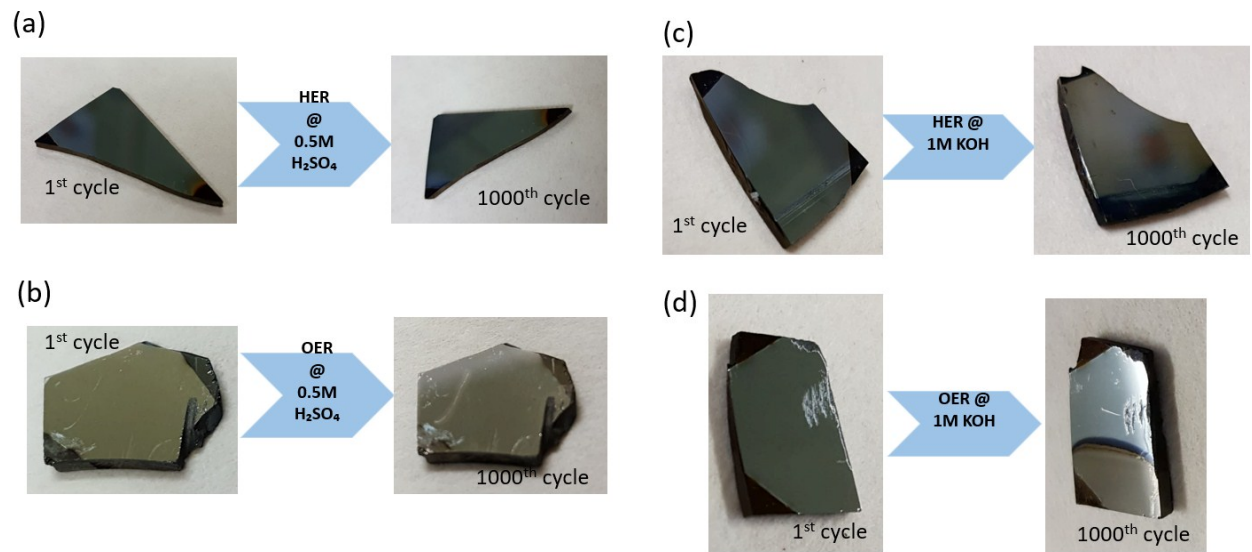


Fig. S15. When supported on VG, Ir can sustain repeated HER and OER cycles in acid (a, b) and alkaline electrolytes (c, d).

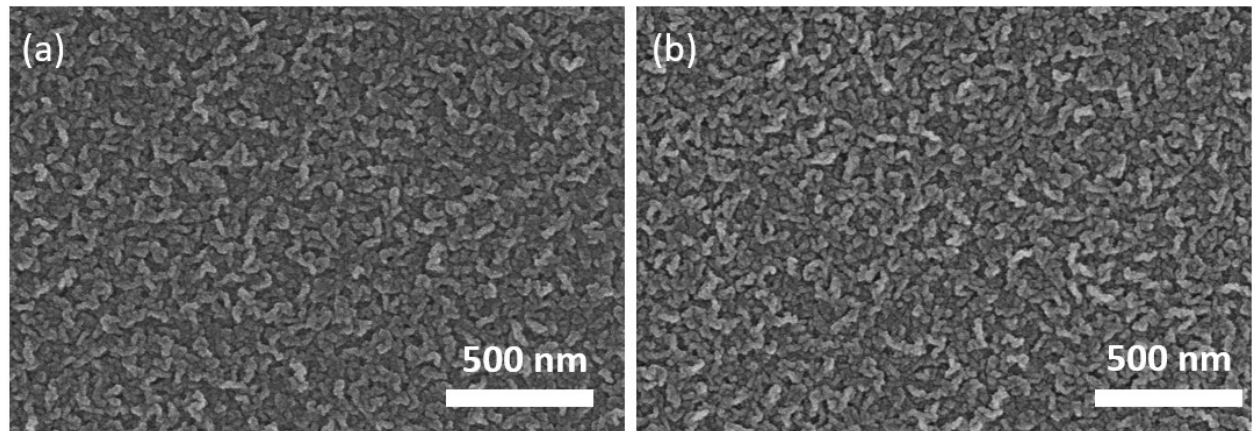


Fig. S16. FESEM images for Ir_VG after 300 CV cycles in acid (a) and alkaline (b). Both imply a bit swollen edges of VG after a long term interaction with acid/alkaline (compared to Fig. S1d).

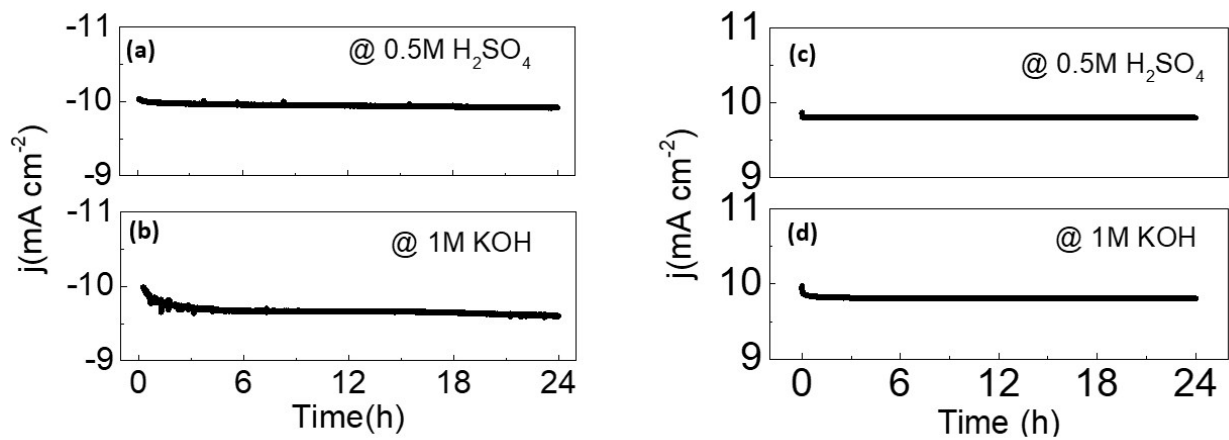


Fig. S17. Stability of Ir_VG for HER and OER: Ir_VG hybrid remains very stable over 24 hours in harsh reaction condition. A steady current density of 10 mA/cm^2 in HER was sustained at low overpotential 47 mV (in acid) and 17 mV (in alkaline) (fig a, b). Ir_VG is also stable in slower OER where a current density of 10 mA/cm^2 was achieved for 24 hours with negligible loss at overpotential of 300 mV (in acid) and 320 mV (in alkaline) (fig c, d).

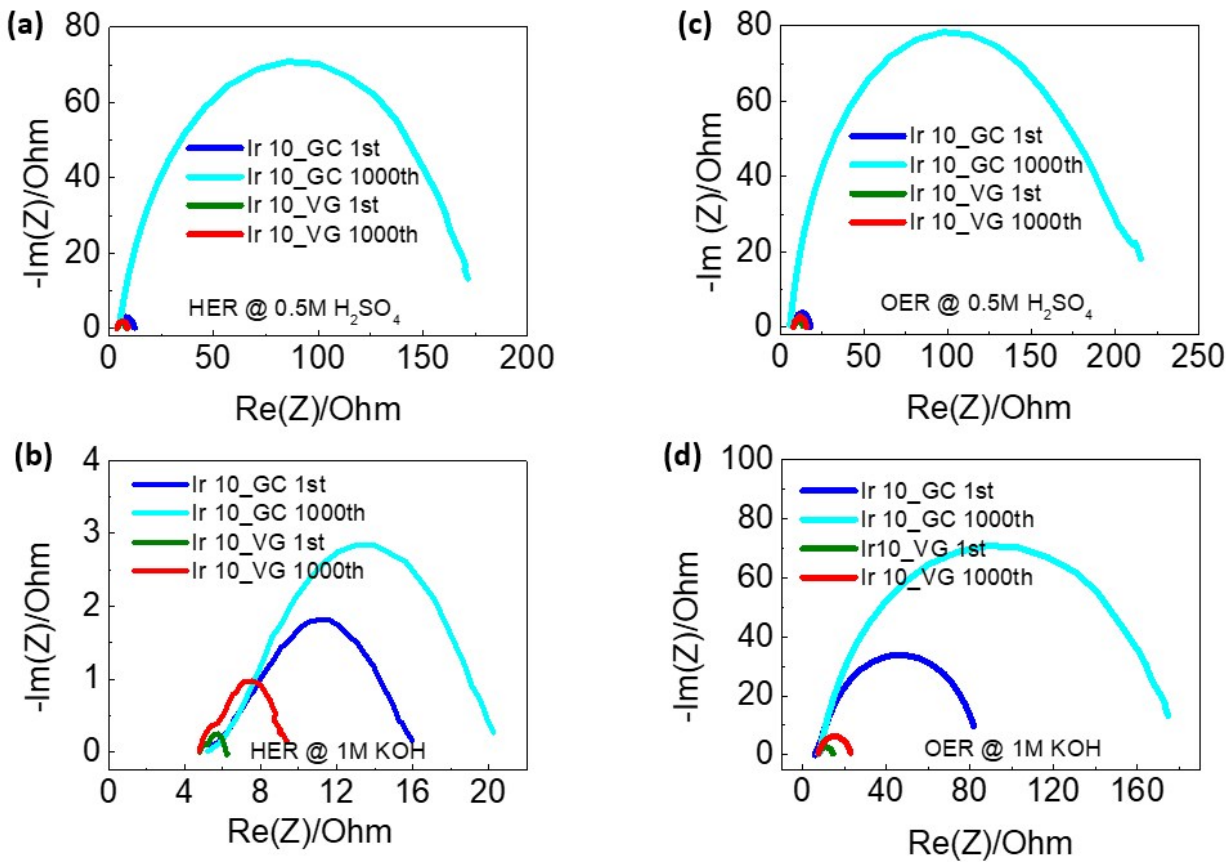


Fig. S18. Comparison of corrosion between Ir_VG and Ir_GC in HER and OER: Ir_GC dissolves during the reaction reflected on its larger charge transfer resistance after 1000 HER/OER CV cycles. The strong adhesion between metallic Ir and graphene nano sheet makes Ir_VG more stable and robust in all four reaction environments. Ir_VG shows almost similar charge transfer resistance before/after 1000 cycles in HER (a, b) and OER (c, d). On contrary, the significant increment of charge transfer resistance of Ir_GC can be an indirect detection of dissolution.

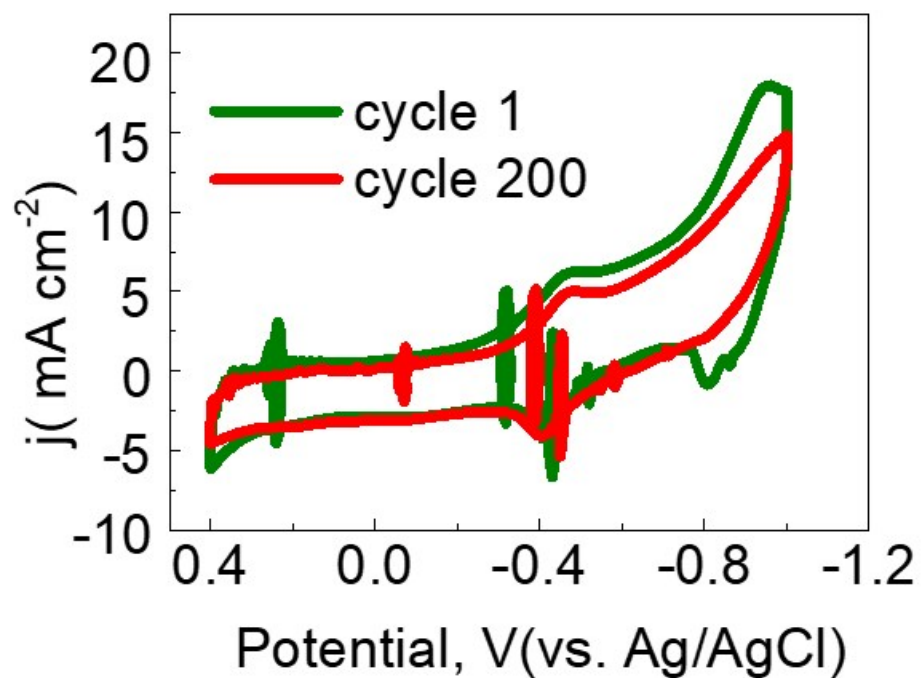


Fig. S19. Confirmation of the existence of metallic Ir after oxidation reaction: CV was performed in 2M NaOH for 200 cycles. The small bump at -0.4 V appears due to the quasi-reversible transition of Ir (III/IV) afterward it reverse to reduction state. After 200 cycles the CV loop remains same indicates that the absence of thick oxide layer.⁴

References:

¹ K. Akbar, S. Hussain, L. Truong, S. B. Roy, J. H. Jeon, S. K. Jerng, M. Kim, Y. Yi, J. Jung and S. H. Chun, *ACS Appl. Mater. Interfaces*, 2017, **9**, 43674–43680.

² J. Kim, P. Shih, K. Tsao, Y. Pan, X. Yin, C. Sun and H. Yang, , *J. Am. Chem. Soc.* 2017, **139**, 12076-12083.

³ J. Liu, Y. Ji, J. Nai, X. Niu, Y. Luo, L. Guo and S. Yang, *Energy Environ. Sci.*, 2018, **11**, 1736-1741.

⁴ N. Arroyo-Currás and A. J. Bard, *J. Phys. Chem. C*, 2015, **119**, 8147–8154.